

Propagation and control of nano-scale, magnetic droplet solitons

M. A. Hoefer,^{1,*} M. Sommacal,^{1,†} and T. J. Silva^{2,‡}

¹*Department of Mathematics, North Carolina State University, Raleigh, North Carolina 27695, USA*

²*National Institute of Standards and Technology, Boulder, Colorado 80305, USA*

(Dated: February 16, 2012)

The propagation and controlled manipulation of strongly nonlinear, two-dimensional solitonic states in a thin, anisotropic ferromagnet is theoretically demonstrated. It has been recently proposed that spin polarized currents in a nanocontact device could be used to nucleate a stationary dissipative droplet soliton. Here, an external magnetic field is introduced to accelerate and control the propagation of the soliton in a damped medium. Soliton perturbation theory corroborated by two-dimensional micromagnetic simulations predicts several intriguing physical effects including the acceleration of a stationary soliton by a magnetic field gradient, the stabilization of a stationary droplet by a uniform control field in the absence of spin torque, and the ability to control the soliton's speed by use of a time varying, spatially uniform external field. Soliton propagation distances approach ten microns in low loss media suggesting that droplet solitons could be viable information carriers in future spintronic applications analogous to optical solitons in fiber optic communications.

Nanomagnetism holds great promise for future spin based information storage and processing technologies [1]. One enabling physical effect is spin torque [2] which imparts angular momentum from a spin polarized current to a magnet. Spin torque forms the basis for tunable microwave nano-oscillators in *confined* nanopillar structures [3] and nanocontacts abutting an *extended* ferromagnet [4]. Most nanopillar dynamics can be reasonably described by single domain modeling [5] with the notable exception of gyrotropic vortex motion [6]. In contrast, nanocontacts enable the excitation of radiating [7, 8] and localized [7] coherently precessing nonlinear wave states. The analysis of solitonic waves in nanocontact systems has predominantly been limited to either the weakly nonlinear regime at threshold [9] or complex micromagnetic simulations [5, 10].

It was recently proposed that a spin torque driven nanocontact could act as a soliton creator in a uniaxial ferromagnet with sufficiently strong perpendicular anisotropy [11]. The resultant strongly nonlinear, coherently precessing state was termed a dissipative droplet soliton, the locally driven/uniformly damped cousin of the two-dimensional (2D), nontopological droplet soliton [12]. Prior numerical computations suggested that the conservative, stationary droplet could be generalized to a propagating solution [13]. This was verified by the construction of a stable, two-parameter family of propagating droplet solutions for the conservative Landau-Lifshitz equation [14]. In this Letter, we use soliton perturbation theory to semi-analytically demonstrate the feasibility of sustaining, moving, and controlling a droplet soliton solely under the action of an external magnetic field. Modulation equations describing the evolution of the soliton's speed and precessional frequency in the presence of damping and a temporally/spatially varying external field are studied and the results are corroborated by 2D micromagnetic simulations. We show that a stationary droplet can be accelerated by a field gradient.

Once in motion, the soliton's speed can be controlled by a spatially uniform, time varying external field. A field gradient due to two nanowires can accelerate a soliton to propagate approximately ten microns in a low loss ferromagnet. Stationary droplets of any allowable frequency can be created from a sufficiently large, localized magnetic excitation, induced by a nanocontact or otherwise, and then stabilized by a linear feedback control field without the use of spin torque. This represents a new mechanism to study magnetic solitons without strong, spin torque induced perturbations. Analogous to optical solitons in fiber optic telecommunications [15], these results show that droplet solitons act as stable, controllable, particle-like, precessing dipoles exhibiting intriguing nonlinear physics and holding potential for spintronic applications.

The model of magnetization dynamics we consider is the Landau-Lifshitz equation [5]

$$\begin{aligned}\frac{\partial \Theta}{\partial t} &= F - \alpha(G + h_0 \sin \Theta), \\ \sin \Theta \frac{\partial \Phi}{\partial t} &= G + h_0 \sin \Theta + \alpha F, \\ F &= \frac{\nabla \cdot (\sin^2 \Theta \nabla \Phi)}{\sin \Theta}, \\ G &= -\nabla^2 \Theta + \frac{1}{2} \sin 2\Theta (1 + |\nabla \Phi|^2),\end{aligned}\tag{1}$$

describing a thin, two-dimensional, unbounded ferromagnet with perpendicular, crystalline anisotropy sufficient to overcome the demagnetizing field so that the steady state is $\Theta \equiv 0$. The magnetization is characterized by its polar and azimuthal angles Θ and Φ , respectively, $\alpha > 0$ is the damping parameter, and $h_0 = h_0(\vec{x}, t)$ is the magnitude of an external magnetic field pointing in the direction normal to the film plane with positive values parallel to the magnetization steady state $\Theta = 0$. Time, space, and fields are normalized by scaled versions of the Larmor frequency $|\gamma|\mu_0 M_s(Q-1)$, exchange length $L_{\text{ex}}/\sqrt{Q-1}$,

and saturation magnetization $M_s(Q - 1)$, respectively, where $Q = H_k/M_s > 1$ is the scaled anisotropy field or quality factor measuring the relative strength of the anisotropy energy to magnetostatic energy. For Co/Ni multilayer anisotropic ferromagnets used in recent experiments [16], the temporal scale and length scale are approximately 27 ps and 17 nm, respectively, and $\alpha \approx 0.01$, $Q \approx 1.25$, $M_s \approx 650$ kA/m. References to dimensional results use these parameter values.

In what follows, we assume that a large amplitude, localized excitation has been nucleated by a spin torque nanocontact [11] or some other means. The rest of this Letter is concerned with the manipulation of this structure in a lossy medium using an external field.

When $h_0 = \alpha = 0$, eq. (1) admits the conservation of spin density $\mathcal{N} = \int (1 - \cos \Theta) d\vec{x}$, momentum $\vec{\mathcal{P}} = \int (\cos \Theta - 1) \nabla \Phi d\vec{x}$, and energy $\mathcal{E}_0 = \frac{1}{2} \int [|\nabla \Theta|^2 + \sin^2 \Theta (1 + |\nabla \Phi|^2)] d\vec{x}$ where all integrals are taken over the plane. Minimizing the energy subject to fixed \mathcal{N} and $\vec{\mathcal{P}}$ leads to a two-parameter family of localized, precessing, stable traveling waves called propagating droplet solitons parameterized by their velocity \vec{V} and frequency in the comoving frame ω [14]. There is a bijective map from $(\mathcal{N}, \vec{\mathcal{P}})$ to the physical parameters (ω, \vec{V}) . Droplet localization requires that the velocity and frequency of the propagating droplet must lie below the spin wave band, enforcing the restriction

$$\omega + |\vec{V}|^2/4 < 1. \quad (2)$$

Typical droplet widths are order one, hence are nanoscale excitations. Stationary droplets with rest frequencies close to zero resemble static circular bubbles which received a great deal of attention in the past [17]. However, typical bubble sizes are much larger. With the inclusion of nonlocal magnetostatic fields, it is predicted that a static bubble will be stable for a 5 nm thick film with a radius above 63 microns [18]. Thus, droplets can be viewed as smaller, dynamic generalizations of the static bubble.

Allowing for weak damping ($\alpha \ll 1$) and a slowly varying magnetic field ($|\nabla h_0|, |\partial_t h_0| \ll 1$) causes the spin density, momentum, and energy to evolve in time. Through the map to (ω, \vec{V}) , we can describe the droplet's adiabatic, particle-like evolution by a time dependence of the droplet's rest frequency and velocity, trajectories in the V - ω phase plane.

Using soliton perturbation theory (see, e.g., [19]), we obtain the following system of modulation equations describing the slow modulation of the spin density and mo-

mentum

$$\begin{aligned} \frac{d\mathcal{N}}{dt} &= -\alpha(\omega + h_0) \int \sin^2 \Theta d\vec{x} \\ &\quad - \alpha \vec{V} \cdot \int \sin^2 \Theta \nabla \Phi d\vec{x}, \end{aligned} \quad (3a)$$

$$\begin{aligned} \frac{d\vec{\mathcal{P}}}{dt} &= -\nabla h_0 \mathcal{N} + \alpha(\omega + h_0) \int \sin^2 \Theta \nabla \Phi d\vec{x} \\ &\quad - \alpha \vec{V} \cdot \int (\nabla \Phi \sin^2 \Theta \nabla \Phi + \nabla \Theta \nabla \Theta) d\vec{x}. \end{aligned} \quad (3b)$$

The energy $\mathcal{E} = \mathcal{E}_0 + \frac{1}{2} \int h_0 (1 - \cos \Theta) d\vec{x}$ is constrained to evolve according to

$$\frac{d\mathcal{E}}{dt} = (\omega + h_0) \frac{d\mathcal{N}}{dt} + (\partial_t h_0 + \vec{V} \cdot \nabla h_0) \mathcal{N} + \vec{V} \cdot \frac{d\vec{\mathcal{P}}}{dt}, \quad (4)$$

thus it is sufficient to evolve eqs. (3) only. The integrals are evaluated with conservative droplets (Θ, Φ) of given spin density $\mathcal{N}(t)$ and momentum $\vec{\mathcal{P}}(t)$ or, equivalently, rest frequency $\omega(t)$ and velocity $\vec{V}(t)$. The field is evaluated along the soliton trajectory $h_0 = h_0(\vec{X}(t), t)$ where $d\vec{X}/dt = \vec{V}$. Similar modulation equations were derived for one-dimensional droplets in [20, 21]. Due to the rotational invariance of eq. (1), we limit further discussion to droplet motion in the x direction so that $\vec{V} = (V, 0)$ and $\vec{\mathcal{P}} = (\mathcal{P}, 0)$ without loss of generality.

In [14], we numerically compute a library of propagating droplets using an iterative technique [22]. These precomputed states are used to numerically solve the modulation equations (3) and to recover $\omega(t)$, $V(t)$. We also perform micromagnetic simulations of the vectorial form of eqs. (1) using a pseudospectral method described in [14]. To recover the micromagnetic solution's speed and frequency, we compute the center of mass $\int \vec{x} (1 - \cos \Theta) d\vec{x} / \mathcal{N}$ and the phase at the center of mass at each time step. The velocity and comoving frequency are then found by differentiation. The rest frequency is recovered by subtracting the local magnetic field $h_0(X(t), t)$. The modulation eqs. (3) represent a low dimensional projection of the magnetodynamics enabling us to bring finite dimensional dynamical systems methods and control theory to bear on the problem. As we demonstrate, the results from modulation theory agree exceptionally well with micromagnetics.

The dynamics of eqs. (3) depend on the magnitude of $|\nabla h_0|/\alpha$. When $|\nabla h_0|/\alpha \gg 1$, the spin density is approximately conserved and the momentum varies. The V - ω phase plane for $h_0 = 0.5 - 0.005x$ and $\alpha = 0.001$ pictured in Fig. 1(a) closely resembles trajectories of constant spin density shown in [14]. The stationary droplet is accelerated while the rest frequency decreases, representing a transfer of the effective potential energy stored in the precessional motion ω to effective kinetic energy of translational motion V . For the balance $|\nabla h_0|/\alpha = \mathcal{O}(1)$, different dynamics occur. Figure 1(b) depicts trajectories for

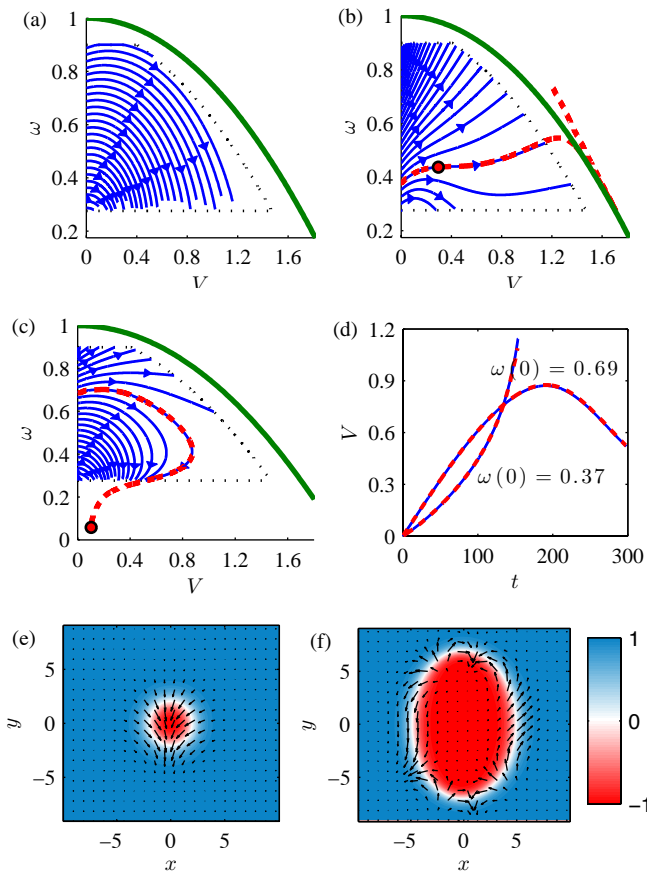


FIG. 1. (a,b,c) Droplet trajectories in the V - ω plane from numerical integration of the modulation equations (3) (solid) and micromagnetics (dashed). The dotted curves correspond to the edges of the precomputed droplet library and the thick, solid parabolic curve is the spin wave band. (a) low loss $\alpha = 0.001$. (b) $\alpha = 0.01$, positive bias field. (c) $\alpha = 0.01$, negative bias field. See text for further details. (d) Droplet velocity time dependence for the solid/dashed trajectories in (b,c). (e,f) Droplet profiles from micromagnetics corresponding to the circles in (b,c), respectively. The gray (color) scale represents the out of plane magnetization $\cos \Theta$ and the arrows represent the in plane magnetization.

the same field as in 1(a) but with $\alpha = 0.01$. The dashed curve depicts the trajectory from micromagnetics with $\omega(0) = 0.37$. The circle on this trajectory corresponds to the droplet shown in Fig. 1(e). The droplet is accelerated and is accompanied by an amplitude decrease until it devolves into a linear spin wave upon reaching the band edge (eq. (2)). The micromagnetic simulation closely matches the adiabatic theory until the band edge is reached and the solution amplitude is very small, after which the droplet ansatz is no longer valid. A plot of $V(t)$ is shown in Fig. 1(d).

During the course of evolution, a droplet can experience deceleration as in Fig. 1(c) with $\alpha = 0.01$ and a negative bias field, $h_0 = -0.5 - 0.005x$. This behav-

ior is reminiscent of Bloch oscillations predicted for one-dimensional droplets in [21]. In the 1D case, the soliton oscillates under a constant force. We have not observed this behavior with our micromagnetic simulations nor modulation theory. Instead, micromagnetic simulations reveal the formation of local, topological structure including vortex/anti-vortex pairs and what appears to be switching of the magnetization to the inverted, $\Theta \equiv \pi$ state, corresponding to $(V, \omega) = (0, 0)$ as shown in Fig. 1(f).

In addition to the dynamics of Fig. 1 for constant field gradient, we have also simulated droplet acceleration due to the field generated by two current-carrying nanowires in the plane of the film with current in the same direction and a stationary droplet nucleated in between them [23]. For the moderate damping case, $\alpha = 0.01$, the droplet is predicted to travel up to $3 \mu\text{m}$ in about 30 ns for 15 mA current in each wire with a $3.3 \mu\text{m}$ wire separation. Top speeds can approach 600 nm/ns . In the low loss case, $\alpha = 0.001$, the droplet can propagate about $10 \mu\text{m}$ in 70 ns for a 10 mA current with a $10.3 \mu\text{m}$ wire separation.

The remaining regime when $|\nabla h_0|/\alpha \ll 1$ is now investigated. We focus on the case of a uniform and static magnetic field, assuming that a propagating droplet has been created. In Fig. 2, solution of the modulation system (3) reveals the *acceleration* of a propagating droplet due to damping when the magnetic field is zero or positive. When the field is sufficiently negative, the droplet can experience deceleration and then acceleration as its amplitude decays. This counter-intuitive droplet acceleration due to damping was predicted for 1D droplets in the absence of a magnetic field [20]. For negative fields, the magnet undergoes a complete reversal to the $(V, \omega) = (0, 0)$ state for initial droplets with parameters lying below a separatrix (see Fig. 2(c)). The switching separatrix corresponds to the stable manifold of the fixed point $(V, \omega) = (0, -h_0)$. Linearization of eqs. (3) around this fixed point results in the eigenvalues

$$\left(\frac{-\int \sin^2 \Theta d\vec{x}}{\partial_\omega \mathcal{N}}, \quad \frac{-\int \Theta_x^2 d\vec{x}}{\partial_V \mathcal{P}} \right), \quad (5)$$

evaluated at the fixed point. Since $\partial_\omega \mathcal{N} < 0$ [12] and $\partial_V \mathcal{P} > 0$ for stationary droplets, the fixed point is a saddle. The switching separatrix from modulation theory accurately resolves the micromagnetic dynamics as evidenced by the close agreement in Fig. 2(c) for trajectories starting very close to the separatrix. It is the existence of this switching separatrix for negative bias field that led to the differing phase plane trajectories in Figs. 1(b) and (c). By changing the external field, the switching separatrix moves, suggesting a mechanism to stabilize a stationary droplet at the saddle point $(V, \omega) = (0, -h_0)$ by use of feedback control.

The nucleation of a stationary droplet by a spin torque driven nanocontact has been theoretically demonstrated [11]. The droplet, which would otherwise decay due

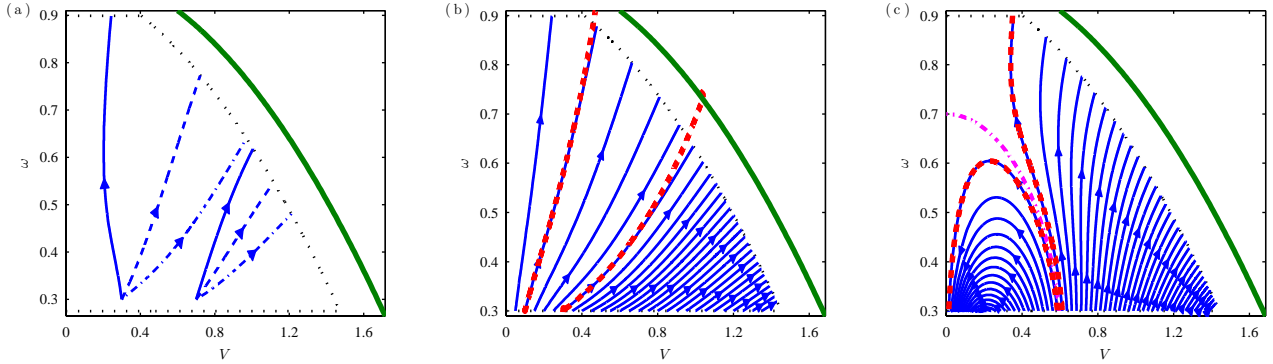


FIG. 2. Droplet trajectories with uniform, static magnetic field and $\alpha = 0.01$. (a) Modulation solution showing acceleration or deceleration of a propagating droplet due to damping and $h_0 = -0.4$ (solid), $h_0 = 0$ (dashed), and $h_0 = 0.9$ (dash-dotted). (b) $h_0 = 1$. (c) $h_0 = -0.7$. In (b) and (c), the dashed curves are micromagnetic simulations. In (c), the dash-dotted curve is the separatrix between the switched state $(V, \omega) = (0, 0)$ and spin wave states.

to damping, is sustained by a balance between localized driving and uniform damping. However, the current induced Oersted field strongly perturbs the stationary droplet from its ideal, symmetric structure, leading to phase variations and potentially a drift instability whereby the droplet is ejected from the nanocontact [11]. Furthermore, canting of the polarization layer is required to obtain an ac electrical signal via giant magnetoresistance leading to symmetry breaking of the spin torque term and further complexity. We propose a simple alternative stabilizing mechanism that avoids these difficulties: a closed-loop, spatially uniform control field. The stationary droplet saddle point $(V, \omega) = (0, \omega_*)$ for $h_0 = -\omega_*$ is altered to an attractor by introducing the linear feedback control

$$h_0(t) = -\omega_* + g[\omega_* - \omega(t)], \quad g > 1, \quad (6)$$

with gain g and bias $-\omega_*$. Stability analysis and numerical computations demonstrate that $(V, \omega) = (0, \omega_*)$ with the control field (6) is a global attractor [23]. We have also performed micromagnetic simulations incorporating the feedback control law (6). Quite generic, localized, large amplitude initial conditions lead to relaxation to the stationary droplet with $\omega = \omega_*$. Simulations showed droplet locking with a 2 ns control field response time [23]. This suggests that any sufficiently large, localized excitation created by spin torque or other means can be deformed into a stationary droplet of choice solely with the use of an external, spatially uniform magnetic field.

In the presence of damping and a constant magnetic field, a propagating droplet is either accelerated or decelerated (recall Fig. 2). A time varying, spatially uniform open loop control field can be used to stabilize the droplet's speed. We compute the field required to maintain constant speed in the modulation equations (3) and use this field profile in micromagnetic simulations. Remarkably, the control field from modulation theory leads

to accurate control of the droplet's speed in the full micromagnetic simulation [23].

We have demonstrated that droplets propagating in a realistic, damped ferromagnet can be sustained, accelerated, and controlled by use of only an external magnetic field. Their robustness and controllability hold promise for future spintronic applications.

* mahoefer@ncsu.edu; <http://www4.ncsu.edu/~mahoefer/>

† msommac@ncsu.edu

‡ silva@nist.gov

- [1] S. Bader and S. Parkin, *Ann. Rev. Cond. Mat. Phys.*, **1**, 71 (2010); J. Lau and J. Shaw, *J. Phys. D: Appl. Phys.*, **44**, 303001 (2011).
- [2] J. C. Slonczewski, *J. Magn. Magn. Mater.*, **159**, L1 (1996); L. Berger, *Phys. Rev. B*, **54**, 9353 (1996).
- [3] J. Katine and E. E. Fullerton, *J. Magn. Magn. Mater.*, **320**, 1217 (2008).
- [4] T. Silva and W. Rippard, *J. Magn. Magn. Mater.*, **320**, 1260 (2008).
- [5] D. Berkov and J. Miltat, *J. Magn. Magn. Mater.*, **320**, 1238 (2008).
- [6] X. W. Yu, V. S. Pribyl, Y. Acremann, A. A. Tulapurkar, T. Tylliszczak, K. W. Chou, B. Bräuer, Z. Li, O. J. Lee, P. G. Gowtham, D. C. Ralph, R. A. Buhrman, and J. Stöhr, *Phys. Rev. Lett.*, **106**, 167202 (2011).
- [7] S. Bonetti, V. Tiberkevich, G. Consolo, G. Finocchio, P. Muduli, F. Mancoff, A. Slavin, and J. Åkerman, *Phys. Rev. Lett.*, **105**, 217204 (2010).
- [8] V. E. Demidov, S. Urazhdin, and S. O. Demokritov, *Nat. Mater.*, **9**, 1476 (2010); M. Madami, S. Bonetti, G. Consolo, S. Tacchi, G. Carlotti, G. Gubbiotti, F. B. Mancoff, M. A. Yar, and J. Åkerman, *Nat. Nano.*, **6**, 635 (2011).
- [9] A. Slavin and V. Tiberkevich, *Phys. Rev. Lett.*, **95**, 237201 (2005).
- [10] D. V. Berkov and N. L. Gorn, *Phys. Rev. B*, **76**, 144414

- (2007); G. Consolo, B. Azzerboni, G. Gerhart, G. A. Melkov, V. Tiberkevich, and A. N. Slavin, *ibid.*, **76**, 144410 (2007).
- [11] M. A. Hoefer, T. J. Silva, and M. W. Keller, *Phys. Rev. B*, **82**, 054432 (2010).
- [12] A. M. Kosevich, B. A. Ivanov, and A. S. Kovalev, *Pis'ma Zh. Eksp. Teor. Fiz.*, **25**, 516 (1977); *Phys. Rep.*, **194**, 117 (1990).
- [13] B. Piette and W. J. Zakrzewski, *Physica D*, **119**, 314 (1998).
- [14] M. A. Hoefer and M. Sommacal, (2011), arXiv:nlin.PS/1111.2310.
- [15] L. F. Mollenauer and J. P. Gordon, *Solitons in optical fibers* (Academic Press, New York, 2006).
- [16] W. H. Rippard, A. M. Deac, M. R. Pufall, J. M. Shaw, M. W. Keller, S. E. Russek, G. E. W. Bauer, and C. Serpico, *Phys. Rev. B*, **81**, 014426 (2010); S. M. Mohseni, S. R. Sani, J. Persson, T. N. Anh Nguyen, S. Chung, Ye. Pogoryelov, and J. Åkerman, *Phys. Status Solidi RRL*, **5**, 432 (2011).
- [17] F. H. D. Leeuw, R. V. D. Doel, and U. Enz, *Rep. Prog. Phys.*, **43**, 689 (1980).
- [18] A. A. Thiele, *J. Appl. Phys.*, **41**, 1139 (1970).
- [19] Y. S. Kivshar and B. A. Malomed, *Rev. Mod. Phys.*, **61**, 763 (1989).
- [20] V. G. Bar'yakhtar, B. A. Ivanov, T. K. Soboleva, and A. L. Sukstanskii, *Sov. Phys. JETP*, **64**, 857 (1986).
- [21] A. M. Kosevich, V. V. Gann, A. I. Zhukov, and V. P. Voronov, *JETP*, **87**, 401 (1998); I. M. Babich and A. M. Kosevich, *Low Temp. Phys.*, **27**, 35 (2001).
- [22] The precomputed droplet library consists of accurately resolved solitons with parameters (V, ω) lying in the set $\{(V, \omega) \mid 0 \leq V \leq 2\sqrt{1 - \omega} - 0.25, 0.275 \leq \omega \leq 0.95\}$ [14].
- [23] See EPAPS Document No. for a description of the nanowire experiments, simulations and details of droplet stabilization and speed control.

ADDITIONAL MATERIAL FOR “PROPAGATION AND CONTROL OF NANO-SCALE, MAGNETIC DROPLET SOLITONS”

ACCELERATING DROPLETS WITH NANOWIRES

Figure 3 depicts the acceleration of a nucleated droplet by means of two in-plane nanowires. The current induced Oersted fields lead to a negative magnetic field gradient that accelerates the droplet. The modulation system, eq. 3, enables a much larger investigation of parameter space than micromagnetic simulations. The simulations incorporate the Oersted field due to two infinite wires with 150 nm diameters and varying separation. Stationary droplets with varying frequencies are assumed to be nucleated 300 nm from the center of the left wire and allowed to propagate until either reaching the second wire or the soliton center of mass attains the value $m_z = 0.5$.

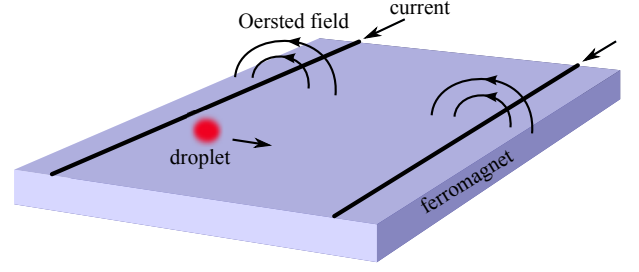


FIG. 3. Droplet acceleration by current flowing through two nanowires.

STATIONARY DROPLET STABILIZATION

A stationary droplet nucleated by a spin torque driven nanocontact experiences significant perturbations due to the Oersted field and canting of the applied field and fixed layer orientation that can lead to a drift instability [11]. To avoid these difficulties, we propose a stabilization mechanism based on linear feedback that turns the stationary droplet saddle point $(V, \omega) = (0, \omega_*)$ for $h_0 = -\omega_*$ into a stable fixed point via

$$h_0(t) = -\omega_* + g[\omega_* - \omega(t)], \quad g > 1. \quad (6)$$

This control could be implemented using a small amplitude (sub-threshold) dc current applied to a trilayer nanocontact with a canted fixed layer resulting in a measurement of $\Omega = \omega + h_0$ with negligible spin torque and Oersted field effects. The goal is to drive Ω to zero. With such a control law, linearization of eq. 3 around the fixed point results in the eigenvalues

$$\left(\frac{-(1-g) \int \sin^2 \Theta d\vec{x}}{\partial_\omega \mathcal{N}}, \quad -\frac{\int \Theta_x^2 d\vec{x}}{\partial_V \mathcal{P}} \right). \quad (7)$$

Since $\partial_\omega \mathcal{N} < 0$ and $\partial_V \mathcal{P} > 0$ [14], when $g > 1$ both eigenvalues are negative and the fixed point is linearly stable. This proves linear (spectral) stability.

We numerically observe that the fixed point is a global attractor in Fig. 4. Figure 4(a) shows the relaxation of the frequency to $\omega_* = 0.5$ for stationary droplets. Figure 4(b) shows that phase perturbations leading to droplet propagation decay in time hence the drift instability has been removed. The gain g determines the relaxation rate to the fixed point with larger values leading to faster relaxation. The constraint $h_0 > -1$ is required in order to avoid spontaneous magnetization reversal in the far field. This limits the choice of the gain to

$$g(\omega_* - \omega(t)) > -1 + \omega_*. \quad (8)$$

If $V(0) = 0$, and the control law (6) is assumed, then eq. (3) simplifies to

$$\frac{d\omega}{dt} = \alpha \frac{(1-g)(\omega_* - \omega)}{\partial_\omega \mathcal{N}} \int \sin^2 \Theta d\vec{x}, \quad (9)$$

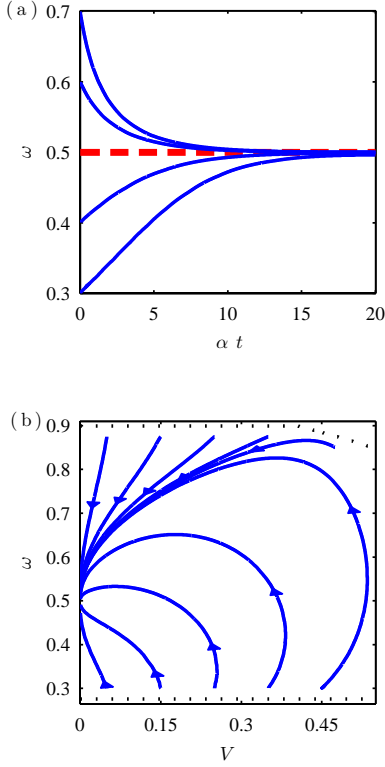


FIG. 4. Stabilization of a stationary droplet with $\omega_* = 0.5$ by the linear feedback control law (6) with $a = 2$. (a) Stationary droplet relaxation. (b) Trajectories in the V - ω plane.

with $V(t) \equiv 0$. Since $\partial_\omega \mathcal{N} < 0$ [12] and $g > 1$, we observe that $\omega = \omega_*$ is a global attractor for fixed $V(t) = 0$ with $\omega(t)$ relaxing monotonically to ω_* . This implies that for $\omega(0) < \omega_*$, inequality (8) will be satisfied for any $g > 1$. However, when $\omega(0) > \omega_*$, then one must choose g such that $1 < g < (1 - \omega_*)/(\omega(0) - \omega_*)$. For small amplitude excitations with $\omega(0)$ close to 1, g will be very close to 1. Thus there is a trade-off between the relaxation time and the stability of the ferromagnet.

We have also performed micromagnetic simulations of the vectorial form of the Landau-Lifshitz equation (1) incorporating the feedback control law (6). We begin the computation with an asymmetric, localized initial condition

$$\Theta(x, y, 0) = Ae^{-(x/w_x)^2 - (y/w_y)^2}, \quad \Phi(x, y, 0) = 0, \quad (10)$$

with $A = 2.7$, $w_x = 2.3$, $w_y = 3$. Equation (1) is evolved with the spatially uniform field (6) where $\omega_* = 0.4$, $\alpha = 0.01$, $g = 3$. We “measure” $\Omega(t) = \omega(t) + h_0(t)$ by averaging the in-plane magnetization orientation over the unit disk to obtain an average phase $\bar{\Phi}(t)$. This models the nanocontact measurement technique suggested. Then, $\Omega(t) = \frac{d\bar{\Phi}}{dt}(t)$. We perform computations with

differing bandwidths or update times so that $h_0(t)$ is updated periodically. Figure 5 depicts the evolution of the

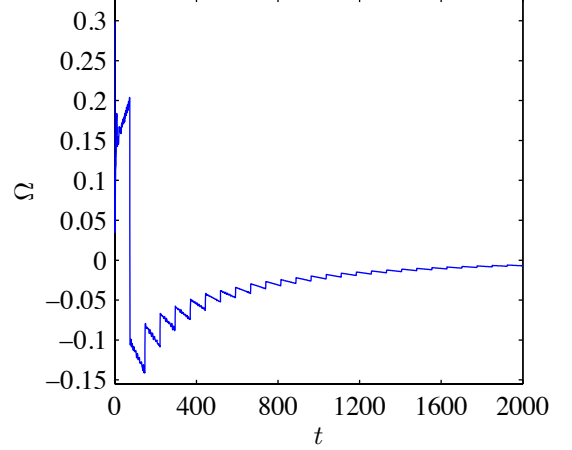


FIG. 5. Micromagnetic simulation giving the spatially averaged magnetization frequency due to the control field (6), $\omega_* = 0.4$, $g = 3$, $\alpha = 0.01$, and an update time of 74. The droplet is locked when $\Omega = 0$.

total frequency $\Omega(t)$ with a field update time of 74 which translates to 2 ns or a 500 MHz bandwidth for perpendicular magnets used in recent experiments [16]. Because damping drives the dynamics, we expect that the operable control bandwidth is approximately $\alpha|\gamma|\mu_0 M_s(Q-1)$, corresponding to about 400 MHz. This suggests that any sufficiently large, localized excitation created by spin torque or other means can be deformed into a stationary droplet of choice solely with the use of an external, spatially uniform magnetic field.

Physically, this stabilization mechanism balances the switching of a droplet by a sufficiently negative bias field and the decay of a droplet via damping.

DROPLET SPEED CONTROL

In the presence of damping and a constant magnetic field, a propagating droplet is either accelerated or decelerated (recall Fig. 2). A time varying, spatially uniform open loop control field can be used to stabilize the droplet’s speed. For this, we implement an optimization strategy for the modulation equations (3) by stepping forward in time and determining the field $h_0(t)$ that enforces the constraint of constant speed. The resulting field profile is fit to a quintic polynomial (see Fig. 6(b)) and used in a micromagnetic simulation of eq. (1) resulting in the trajectories shown in Fig. 6(a). Remarkably, the control field from modulation theory leads to accurate control of the droplet’s speed in the full micromagnetic simulation.

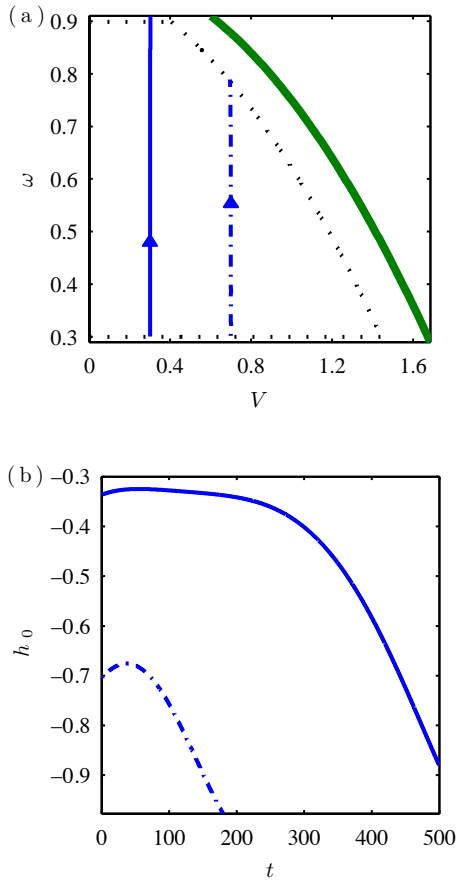


FIG. 6. Open loop control of droplet speed. (a) Two trajectories (solid, dash-dotted) in the V - ω plane from micromagnetic simulations with (b) the corresponding control field (solid, dash-dotted, respectively) determined from the modulation equations (3).